Supplementary Material

Sample fabrication

The experimental samples are built up on conventional 6061-T6 aluminum plates. Fig. S1**(a)** shows the photograph of A_0 wave sample that consists a plate with size 180 cm $\times$ 6 cm $\times$ 0.8 cm, in the x, y and z axes, respectively. x axis is along the propagating direction, y axis is along thickness direction, whereas the z axis is vertical to x-y plane. The plate has thickness 6 cm rather than 0.8 cm. So that the x axis changes from -90 cm to 90 cm, and y axis occupies $0 \sim 6$ cm. Regarding Rayleigh wave sample, the plate thickness becomes 120 cm along y axis, being about 8 times the maximum Rayleigh wavelength of $\sim$ 15.4 cm in this work.

The chiral elastic source, as shown in Fig. S1**(b)**, is installed around center at (x, y) = (0, 1.2 cm). The chiral source constitutes four sub-sources in square lattice with the lattice distance $d = 12$ mm. For each of them, an aluminum rod (green) whose radii $r = 2.25$ mm is firstly fixed by epoxy adhesive (red) to the air hole perforated through aluminum plate (gray), and then two PZT rings (blue) are symmetrically glued by epoxy adhesive to the two laterals of aluminum rod. The PZT rings used here are made of PZT-8 with the outer diameter 10 mm, inner diameter 5 mm, and thickness 1 mm. In this way, electrical signals generated upon the PZT rings can transpose forces to the aluminum rods into breathing vibration and then generates elastic waves in the substrate solid structures. However, due to the efficient generation of breathing mode, the aluminum rod cannot be long along the z axis, and consequently, the plate size is chosen to be 0.8 cm for both A_0 and Rayleigh waves.

Experimental measurements

The 5-cycled tone burst electrical signals with central frequency f_c are issued from the function generator (RIGOL DG1032z) and amplified by the power amplifier (Aigtek ATA-2022H). Concerning the measurement, the laser Droppler vibrometer (LDV, Polytec vibrometer OFV 2570) is used to record the out-of-plane displacement u_y at any position on the x-z surface. Each measurement comes from the averaging over 256 scans digitized by an oscilloscope (DPO 4102B) at sampling frequency of 100 MHz. This measurement allows for a good signal-to-noise (S/N) ratio.

To obtain SAM of elastic wave along x-z surface, small V-shape grooves with size about 5 mm $\times$ 5 mm were drilled as shown in Fig. S1**(c)**. Each groove has two faces with side length 5 mm, and it brings almost no influence on wave transmission since the size is much smaller than the wavelength of elastic wave in this work. In experiment, we measure only the out-of-plane displacements on the two faces of each groove. Let us label the out-of-plane displacement as u_2 when measured at the right face and as u_1 at the left face. Then, we calculate the in-plane displacement u_x and out-of-plane displacement u_y on the x-z surface for an effective point in between each groove. For simplicity, the effective point is marked as the central point of each groove on x-z surface, to be x = ±45 cm in the end. In detail, for the small grooves on front surface y = 0, the u_x and u_y can be obtained as u_x= $u_1 cos(\theta_1) - u_2 cos(\theta_2)$ and $u_y = -u_1 sin(\theta_1) - u_2 sin(\theta_2)$, while for grooves on back surface y = 6 cm only in A_0 wave system, the $u_x = u_1 cos(\theta_1) - u_2 cos(\theta_2)$ and $u_y = u_1 sin(\theta_1) + u_2 sin(\theta_2)$. The value of angle θ_1 and θ_2 is 45^o.

Simulation of elastic spin for chiral Rayleigh wave

The simulation results about the spin-up/down excitation in Rayleigh wave are shown in Fig. S2. Here, We use 2D elastic model in Comsol to illustrate the spin-momentum locking, and the source here is the same as the four-point source demonstrated in Fig. 1 (b) in the main text. Although the profile of displacement polarization on both sides are similar, the propagation direction is different. Hence, the rotation direction of local displacement polarization are opposite between the left and right sides. As such, the spin-up (rep. spin-down) source only excite Rayleigh mode in left (resp. right) side, while the wave mode in the other side is forbidden due to the mismatching in SAM.

Observation of elastic spin for A_0 wave upon spin-down source

The spin-down source with central frequency f_c = 14 kHz was generated. Then, we measured the u_y of both the left-going ($x < 0$) and right-going waves ($x > 0$) every 1 cm, on the x-z surfaces at y = 0 and y = 6 cm, respectively. Fig. S3**(a)** shows the normalized 2D-FFT components of u_y recorded at back surface y = 6 cm, magnifying a primary spot well located on the right A_0 branch, i.e. the domination of right-going A_0 wave over the left-going one. At the same time, the components of S_0 waves are minor. The FFT component of u_y of each point measured on back surface y = 6 cm, as shown in Fig. S3**(b)**, also shows the prior generation of rightward A_0 wave, being consistent with the numerical results in Fig. S3**(c)**. Fig. S3**(d)** shows the experimental profiles of u_x and u_y at the point x = 45 cm and y = 6 cm, which leads to the anti-clockwise rotation of $\boldsymbol{u}$ and the positive $\boldsymbol{S}$ for the rightward A_0 wave. The results obtained on front surface y = 0, shown in Figs. S3**(e)** - **(g)**, feature the same rightward A_0 wave, but demonstrate the negative SAM at x = 45 cm and y = 0, being just opposite to the one on surface y = 6 cm.

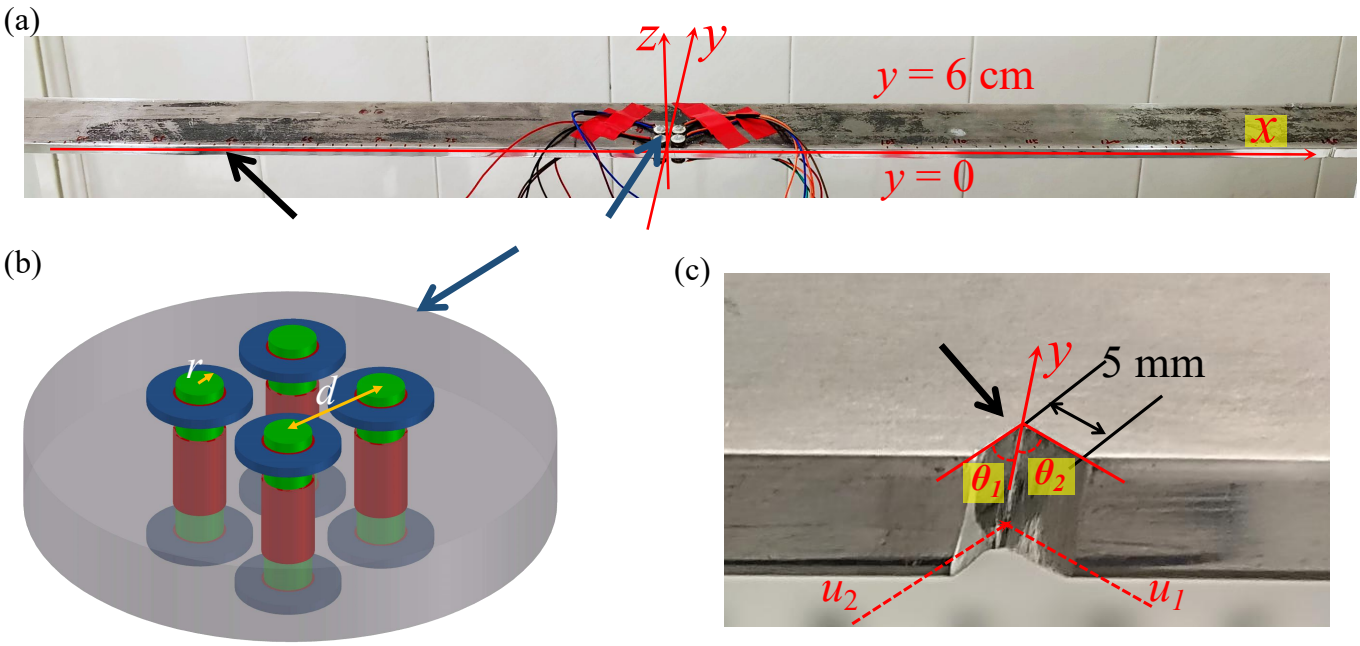

FIG. S1. **(a)** Photograph of experimental sample for A_0 wave where a chiral elastic source installed around point at (x, y) = (0, 1.2 cm). **(b)** Schematic of chiral elastic source built up by inserting four group of PZTs with distance $d = 12$ mm. For each group, an aluminum rod (green) with radii $r = 2.25$mm is firstly fixed by epoxy adhesive (red) to the air hole perforated through the aluminum slab (gray), and then two PZT rings (blue) are symmetrically glued by epoxy adhesive to the two laterals of the aluminum rod. **(c)** Photograph of V-shape groove with side length 5 mm which is much smaller than the wavelength in our systems, and the measurement of the out-of-plane displacement on two faces of grooves.

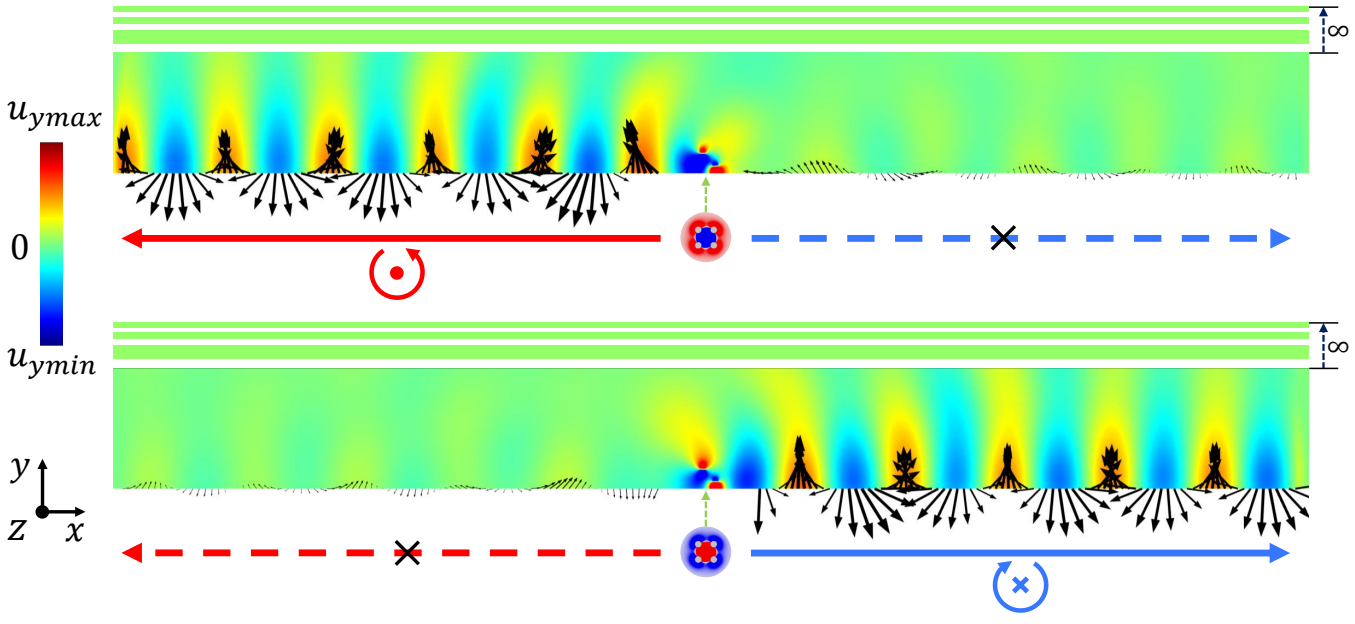

FIG. S2. The spin-momentum locking in Rayleigh wave. Top/bottom panel shows the spin up/down excitation. The magnitude and direction of displacement polarization at the free boundary are shown with black arrows.

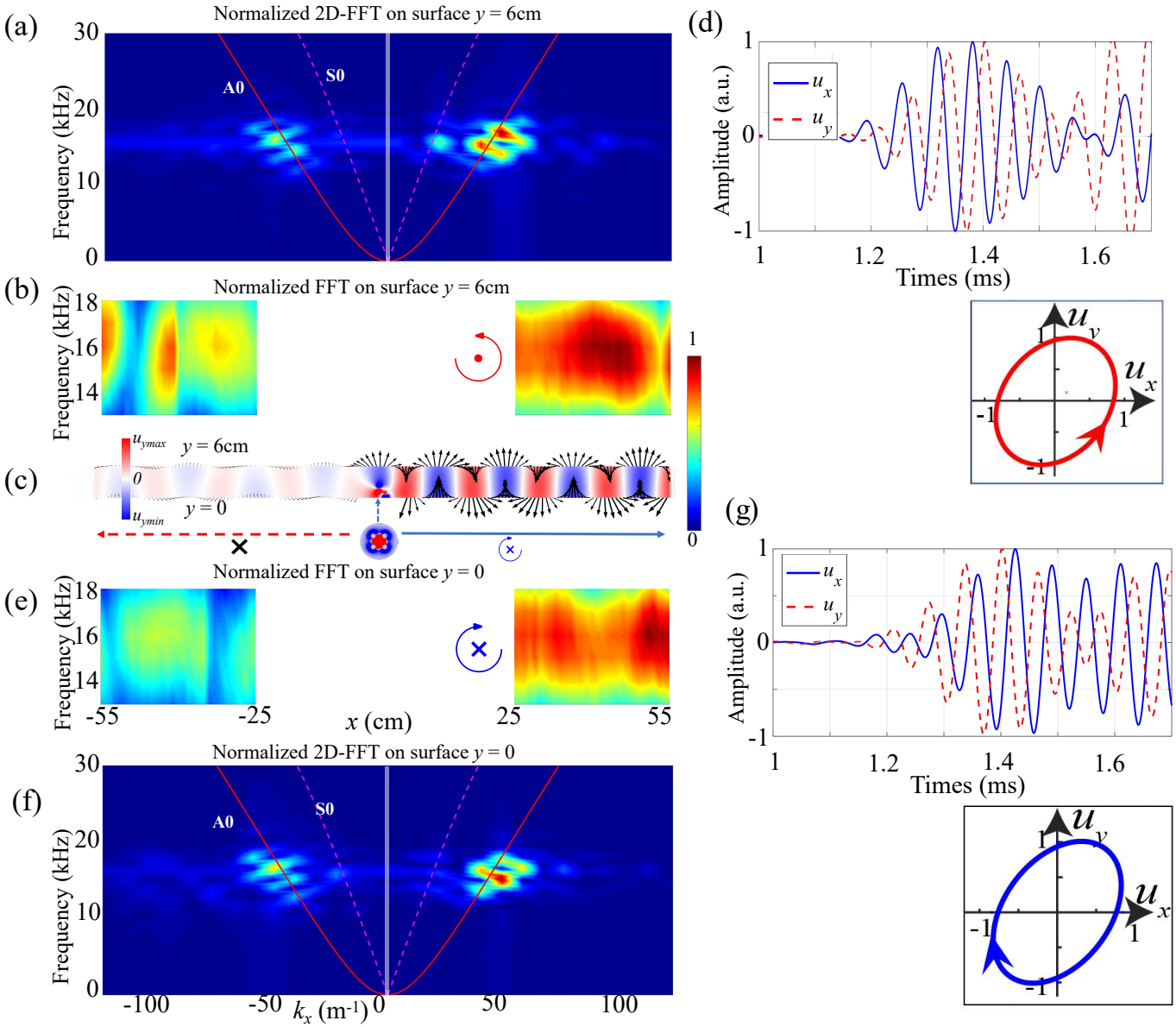

FIG. S3. **Experimental observation of spin for spin-dependent chiral A_0 wave upon the spin-down source at central excitation frequency f_c = 14 kHz.** **(a)** Normalized 2D-FFT component of measured signals on back surface at $y = 6$ cm. Red solid and magenta dash lines present the A_0 and S_0 branches, respectively. Hot spot spreads well over the right branch of A_0 wave. **(b)** Normalized FFT of u_y measured at each position along $x = -55 \sim -25$ cm and $x = 25 \sim 55$ cm every 1 cm on back surface $y = 6$ cm. FFT components shows the rightward wave propagation over leftward one. The rotation of displacement polarization $\boldsymbol{u}$ is anti-clockwise to give the positive SAM at rightward route. **(c)** Simulated A_0 wave propagation with SAM opposite on two surfaces of aluminum plate. **(d)** Time evolution of u_x and u_y at x = 45 cm and y = 6 cm, featuring the anti-clockwise rotation of displacement polarization $\boldsymbol{u}$ for the right-going A_0 wave. **(e)** Normalized FFT of u_y measured along $x = -55 \sim -25$ cm and $x = 25 \sim 55$ cm every 1 cm on front surface $y = 0$. The FFT components are much larger at right side, but the rotation of displacement polarization $\boldsymbol{u}$ is clockwise for the right-going waves. **(f)** Normalized 2D-FFT component of u_y on front surface y = 0. The A_0 wave amplitude is much larger at right branch. **(g)** The experimental profiles of u_x and u_y at x = 45 cm and y = 0, and the related clockwise rotation of displacement polarization $\boldsymbol{u}$ for the right-going A_0 wave.

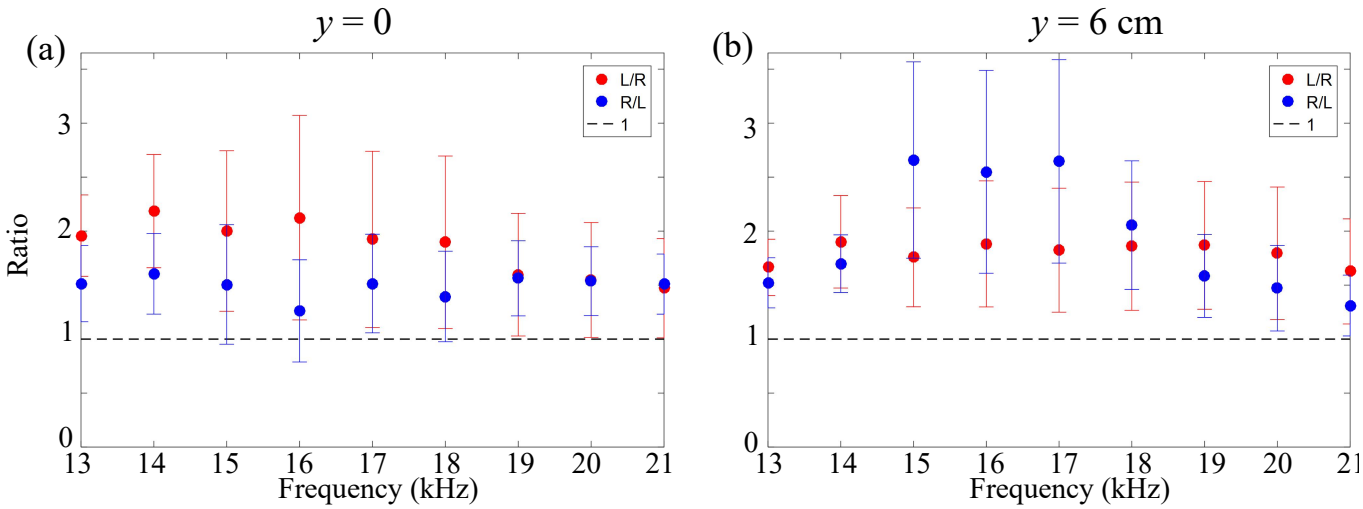

FIG. S4. Average ratios of measured $|u_y|$ of A_0 wave on x-z surfaces at (a) y = 0 and (b) y = 6 cm, within the x = -55 $\sim$ -25 cm and x = 25 $\sim$ 55 cm. In both figures, the red dots are for the $|u_{y(x<0)}/u_{y(x>0)}|$ when using spin-up source while the blue dots stands for $|u_{y(x>0)}/u_{y(x<0)}|$ upon the spin-down source. The bars at each frequency are defined as the average ratio plus and/or subtract standard deviation of ratios derived at every group of points, i.e. $|u_{y(x=-30cm)}/u_{y(x=30cm)}|$.